Open Access Articles

Improved oxidation resistance of organic/inorganic composite atomic layer deposition coated cellulose nanocrystal aerogels

The Faculty of Oregon State University has made this article openly available.
Please share how this access benefits you. Your story matters.

Citation	Smith, S. W., Buesch, C., Matthews, D. J., Simonsen, J., & Conley Jr, J. F. (2014). Improved oxidation resistance of organic/inorganic composite atomic layer deposition coated cellulose nanocrystal aerogels. Journal of Vacuum Science & Technology A, 32(4), 041508. doi:10.1116/1.4882239
DOI	10.1116/1.4882239
Publisher	American Vacuum Society
Version	Version of Record
Terms of Use	http://cdss.library.oregonstate.edu/sa-termsofuse

Improved oxidation resistance of organic/inorganic composite atomic layer deposition coated cellulose nanocrystal aerogels

Sean W. Smith
School of Electrical Engineering and Computer Science, 1148 Kelley Engineering Center, Oregon State University, Corvallis, Oregon 97331

Christian Buesch
Department of Wood Science and Engineering, Oregon State University, 119 Richardson Hall, Corvallis, Oregon 97331

David J. Matthews
School of Electrical Engineering and Computer Science, 1148 Kelley Engineering Center, Oregon State University, Corvallis, Oregon 97331

John Simonsen
Department of Wood Science and Engineering, Oregon State University, 119 Richardson Hall, Corvallis, Oregon 97331

John F. Conley, Jr.[a)]
School of Electrical Engineering and Computer Science, 1148 Kelley Engineering Center, Oregon State University, Corvallis, Oregon 97331

(Received 25 February 2014; accepted 27 May 2014; published 12 June 2014)

Cellulose nanocrystal (CNC) aerogels are coated with thin conformal layers of Al_2O_3 using atomic layer deposition to form hybrid organic/inorganic nanocomposites. Electron probe microanalysis and scanning electron microscopy analysis indicated the Al_2O_3 penetrated more than 1500 μm into the aerogel for extended precursor pulse and exposure/purge times. The measured profile of coated fiber radius versus depth from the aerogel surface agrees well with simulations of precursor penetration depth in modeled aerogel structures. Thermogravimetric analysis shows that Al_2O_3 coated CNC aerogel nanocomposites do not show significant thermal degradation below 295 °C as compared with 175 °C for uncoated CNC aerogels, an improvement of over 100 °C. © *2014 American Vacuum Society*. [http://dx.doi.org/10.1116/1.4882239]

I. INTRODUCTION

Cellulose nanocrystals (CNCs) are high aspect ratio nanoparticles that can be derived from a variety of materials such as plants, algae, and sea animals. Their size varies from 3 to 20 nm in cross section and 50 to 2000 nm in length. CNCs are biocompatible and essentially nontoxic with a strength rivaling aluminum and a modulus surpassing that of carbon steel. Because of these unique properties, CNCs have recently been the subject of a great deal of research exploring a variety of applications ranging from biomedical devices to optical components. They have also been widely proposed as reinforcing fillers in polymers.[1] However, the well-known sensitivity of CNCs to oxidation at low temperatures has limited their ability to be incorporated into polymers, which typically require high temperature processing (>200 °C) in oxygen containing environments.[2] Although application of a thin surface coating might provide oxidation resistance to CNCs, CNCs are typically produced in aqueous solutions and agglomerate or form films upon drying, making coating difficult. Recent work, however, has shown that CNCs can be readily formed into aerogels, which possess a unique microstructure of loosely spaced particles with very high porosity, low density, and high surface area.[1,3] The aerogel morphology allows not only for unique architectures, but also makes available the CNC surface to interaction with process gases, opening the possibility of coating aerogel CNCs with protective thin films. Although coating of such high surface area porous substrates is not possible with standard deposition techniques such as sputtering, evaporation, or traditional chemical vapor deposition (CVD), atomic layer deposition (ALD) is well-suited for the task.[4–8] ALD is a chemical vapor deposition technique in which precursors and reactants are introduced sequentially to the reaction chamber. Deposition takes place via self-limiting surface reactions so that the film builds up one layer at a time, allowing for highly uniform and conformal coating of thin film inorganic oxides over high aspect ratio porous and large surface area structures.[9] ALD coatings have been applied to woven cotton fibers to control wettability[10] and conductivity,[11] and applied to CNC aerogels for a variety of purposes such as to increase biocompatibility,[12] to form a high surface area TiO_2 substrate for dye sensitized solar cells,[13] to create inorganic nanotube aerogels using sacrificial CNC aerogel templates,[14] to form reusable floating oil absorbents,[15,16] and to demonstrate photoselective super-absorbency of water.[17] It has recently been shown that ALD films of Al_2O_3 as thin as 25 nm make excellent moisture permeation barriers.[18] ALD Al_2O_3 films have also been shown to protect other carbon-based structures from oxidation, in one case increasing the oxidation temperature of carbon fibers by 60 °C.[19]

[a)]Electronic mail: jconley@eecs.oregonstate.edu

Redistribution subject to AVS license or copyright; see http://scitation.aip.org/termsconditions. Download to IP: 128.193.163.187 On: Fri, 08 Aug 2014 20:06:11

In this work, ALD is used to deposit conformal Al_2O_3 coatings on CNC aerogels to improve oxidation resistance for incorporation as reinforcing fillers in polymers. Electron probe microanalysis (EPMA) is used to measure the penetration of Al into the aerogel. Scanning and transmission electron microscopy (SEM and TEM) are used to monitor coating conformality and thickness as a function of depth in to the aerogel. To assist interpretation of EPMA, SEM, and TEM data, the penetration depth of the ALD Al_2O_3 film into the CNC aerogel is modeled based on the work of Yanguas-Gil and Elam.[20] Finally, thermogravimetric analysis (TGA) is used to assess the effectiveness of the coatings in preventing oxidation related weight loss.

II. EXPERIMENT

CNCs are prepared from pure cotton cellulose by hydrochloric acid hydrolysis using a previously described method.[21,22] In the first step of this two-step process, comminuted cellulose is subjected to hydrolysis by immersing in 2.5M HCl at 100 °C for ~30 min. The resulting aqueous CNC-containing mixture is then subjected to oxidation, converting the surface C6 primary hydroxyls to carboxylic acids via (2,2,6,6-tetramethylpiperidin-1-yl)oxyl (TEMPO) mediated carboxylation.[23–26] Briefly, 200 ml of 1% CNC suspension is slowly stirred with 140 mg of TEMPO (70 mg/g CNC) and 360 mg of NaBr (180 mg/g CNC). The reaction is initiated by adding an initial aliquot of 6% hypochlorite (NaClO) to the reaction mixture. A *p*H of 10.2–10.5 is maintained by adding dilute NaOH via a *p*H controller for 4 to 8 h. The reaction is quenched with 30–40 ml of ethanol and then purified by dialysis. Carboxylate content on the CNC surface is determined via conductometric titration against 0.05 *N* NaOH. Typical values of carboxylate content are ~1 mmol/g CNC. The surface charge imparted by the carboxylate groups sets up repulsive forces between the colloidal particles that result in a spontaneous and stable dispersion of CNC particles in an aqueous suspension. The prepared CNCs are further processed by carefully layering an organic solvent (acetone) over the aqueous CNC dispersion containing 1.0%–1.5% carboxylated CNCs (solvent: CNC dispersion = 5:1). The solvent is decanted and replaced 3–4 times over the course of 5 days forming a CNC organogel (gel in organic solvent). After a dry organogel (all residual water replaced with acetone) is obtained, the solvent is removed by soaking the organogel in liquid CO_2 at 1200 psi and 25 °C for 18–24 h. The vessel is then slowly vented and refilled every 30 min ($\Delta P = \pm 200$ psi, 3×), followed by soaking in supercritical CO_2 (1500 psi, 35 °C) for 1 h, after which the vessel is depressurized at less than 100 psi/min. A highly porous, white solid is obtained, as shown in Fig. 1(a). Typical densities of the aerogels are between 0.05 g/cm^3 and 0.1 g/cm^3.

Al_2O_3 films are deposited on approximately $10 \times 5 \times 5$ mm pieces of CNC aerogel via ALD in a Arradiance Gemstar^{TM} flow-through hot wall reactor at either 80 °C or 150 °C using trimethylaluminum (TMA, $Al(CH_3)_3$) and water as reactants. To reduce residual absorbed water, all aerogels are baked out in the deposition chamber at 150 °C under approximately 1 Torr N_2 for 24 h prior to ALD. Samples baked out at 80 °C are found to be fractured and blackened during ALD, presumably from TMA reacting with residual water.

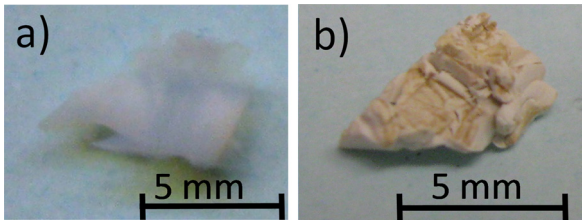


FIG. 1. (Color online) Photographs of (a) uncoated and (b) ALD coated CNC aerogels.

A typical ALD cycle for coating a planar surface consists of four basic steps: (1) a pulse of the first reactant is introduced, which reacts with functional groups on the substrate surface; (2) reaction products as well as excess and physisorbed reactants are purged away with an inert gas (typically N_2); (3) a pulse of the second reactant is introduced, which reacts with the chemisorbed layer of the first reactant; (4) excess reactant and reaction products are again purged away with inert gas.[9] These steps are repeated to deposit a film with the desired thickness. In order to coat a high aspect ratio structure such as an aerogel, the four step sequence described above must be modified. After steps (1) and (3), additional exposure steps are added during which the substrate is allowed to "soak" in the reactant gas for a period of time prior to the purge step to allow the reactant sufficient time to diffuse into and out of the porous substrate. To enable this, a stop valve to the vacuum pump is closed prior to reactants being pulsed into the chamber. Similarly, the purge steps are extended to give the excess reactants and reaction products enough time to diffuse out again. Finally, compared to planar substrates, a larger dose of reactants must be used to account for the high surface area of the aerogel.[4–7,14–17] This is accomplished by increasing the reactant pulse times. ALD Al_2O_3 coatings are investigated with respect to ALD pulse time, and exposure and purge time. Depositions of 15, 50, and 272 ALD cycles are used with a range of reactant pulse times (20, 60, 180, 500, 1000, and 2000 ms), and exposure and purge times (30, 120, and 600 s). Note that for all ALD coatings discussed in this work, the exposure and purge times are set equal and thus are given as one value. A typical coated aerogel is shown in Fig. 1(b).

Al_2O_3 film thickness is measured on planar silicon witness samples via ellipsometry, accounting for a thin native oxide. To investigate Al_2O_3 penetration, the penetration of Al atoms into aerogel samples is measured by EPMA using a Cameca SX-100 Electron Microprobe. Al_2O_3 coated aerogel samples are embedded in epoxy (SPURRS, Ted Pella, Inc.), cross sectioned, and then polished prior to EPMA measurements. To examine the microstructure as well as Al_2O_3 penetration, other coated aerogels are cleaved and the fracture surface is examined using either an FEI QUANTA 600F SEM or an FEI NOVA NanoSEM 230 high resolution SEM. To examine coating conformality, TEM images of select coated samples are collected on a FEI Titan 200 kV TEM/STEM.

Redistribution subject to AVS license or copyright; see http://scitation.aip.org/termsconditions. Download to IP: 128.193.163.187 On: Fri, 08 Aug 2014 20:06:11

Weight loss curves of coated and uncoated aerogels are collected in a TA Instruments TGA Q500 thermogravimetric analyzer (TGA). TGA is performed on small whole (unbroken) pieces of coated aerogel with masses of 5–10 mg [Fig. 1(b)]. All TGA measurements are conducted in air with a heater ramp rate of 10 °C/min. Data are plotted both as weight percent versus temperature and log differential weight % versus temperature. Differential weight % data are averaged over seven data points to reduce noise (for the sample and sweep rates used, there is less than a 1 °C change in temperature over seven data points).

The TMA penetration depth in the CNC aerogels is modeled in Matlab based on the work of Yanguas-Gil and Elam,[20] which is based on the model developed by Gordon *et al.*[27] generalized to fit an arbitrary geometry. The CNC fiber structure is approximated as a cubic network of cylinders.[28] The spacing of the cylinders is adjusted to fit SEM observations, either 100 nm or 160 nm center to center. The critical time t_c to coat a feature of length L is given by

$$t_c = A\frac{L^2}{D}\frac{1}{\gamma}\left(1 - \frac{\log(1-c)}{\alpha}\right), \tag{1}$$

where D is the precursor diffusivity, γ is the precursor excess number, α is the Damkohler number, c is the coverage fraction (0.9999 for this model), and A is a correction factor that we have added to account for reaction chamber dependent transport time and assumptions in the model as discussed below. The precursor excess number, γ, represents the ratio of available precursor molecules, N_V, to the number of available reaction sites, N_S, and is given by

$$\gamma = \frac{N_V}{N_S} = \frac{V}{S}n_0 s_0, \tag{2}$$

where V is unfilled volume of our aerogel model, S is the surface area, n_0 is the precursor concentration at the aerogel surface, and s_0 is the surface area of one adsorbed precursor molecule. Finally, α represents the ratio of the diffusion time, t_{diff}, to the reaction time, t_{reac}, and is given by

$$\alpha = \frac{t_{\text{diff}}}{t_{\text{reac}}} = \frac{1}{4}L^2\bar{s}\frac{v_{\text{th}}}{D}\beta_0, \tag{3}$$

where $\bar{s}$ is the surface area per unit volume, v_{th} is the root mean square thermal velocity of a precursor molecule, and β_0 is the reaction probability. β_0 is assumed to be 1 for ALD by TMA and H_2O.[27]

In our model, t_c is set equal to the exposure time and Eqs. (1)–(3) are used to solve for L, giving the expected penetration depth of each pulse. As seen in Eq. (1), t_c includes the planar saturation time plus an aspect ratio dependent term. Note that the model does not include the time required to transport the TMA from the ALD valve to the sample surface, which may be significant and varies with reactor design.[20] In addition, a constant pressure during deposition is assumed, but the actual reactor pressure increases gradually during the exposure step as the pump line is closed and nitrogen still flows into the chamber. To account for variations in transport time and reactor pressure, a correction factor of A = 30 is applied to fit the modeled profile to SEM measured profiles.

Equations (1)–(3) are used to generate the relationship between the aerogel penetration distance, L, and the coated fiber radius, r_{cyl}, at depth L for a given set of pulse and exposure times. The ratio V/S is calculated from r_{cyl}, and the value n_0 is dependent upon pulse time. The L versus r_{cyl} relationship is used to model the ALD penetration profile as a function of ALD cycles for a given average growth per cycle (GPC) and initial CNC fiber radius. The GPC used for modeling is based on the planar silicon witness coupons included in each aerogel run, and the initial CNC fiber radius is determined from TEM. Changing the deposition temperature from 150 °C to 80 °C is found to have little impact on the modeled profiles.

To generate model ALD thickness profiles a sharp boundary is assumed to exist between the coated and uncoated regions for each ALD pulse. For all areas of the aerogel less than distance L from the surface, the GPC is added to the thickness of the coating during each cycle. For depths beyond L, no thickness is added. As the CNC fibers (cylinders in the model) are coated, they increase in radius and reduce the porosity, decreasing the V/S ratio of the cylinder network and increasing t_c, reflecting the reduced ability of TMA to penetrate the network. Assuming that the buildup of film thickness throughout a deposition is sufficient to cause a reduction in L, the final oxide thickness profile consists of three regions: (1) Near the surface, defined by the minimum penetration depth, L_{min}, the coating thickness is determined by the number of cycles times the GPC. We refer to this region as cycle-limited. (2) Between L_{min} and the initial penetration depth, L_{max}, ALD penetration is limited by the decreasing porosity of the film, so that the coating thickness transistions from the maximum thickness in the surface region to zero. We refer to this region as penetration limited. (3) No ALD pulses reach beyond L_{max}, so deeper portions of the aerogel remain uncoated.

III. RESULTS AND DISCUSSION

A. Imaging and deposition modeling

A TEM cross section of coated aerogel taken near the aerogel surface is shown in Fig. 2. This sample is coated with 50 cycles of Al_2O_3 at 80 °C with 500 ms pulses and 120 s exposure and purge times. The dark, hollow looking tubes in the image show a conformal ALD Al_2O_3 coating surrounding the CNC fibers. In this portion of the sample, the ALD coating is 11 nm thick, and the CNC fibers have an average radius of 4 nm.

Shown in Fig. 3 are cross-sectional EPMA images of CNC aerogels coated at 150 °C with 50 cycles of ALD Al_2O_3. In Fig. 3(a), each ALD cycle consisted of 180 ms pulses with 600 s exposures and purges. There are three distinct regions of Al intensity evident in Fig. 3(a): an outer layer approximately 350 μm deep with high Al counts, an inner layer beyond 350 μm where the Al signal decreases with depth, and an uncoated interior region. Al penetration of at least 550 μm is evident. In preparation for EPMA, the

Redistribution subject to AVS license or copyright; see http://scitation.aip.org/termsconditions. Download to IP: 128.193.163.187 On: Fri, 08 Aug 2014 20:06:11

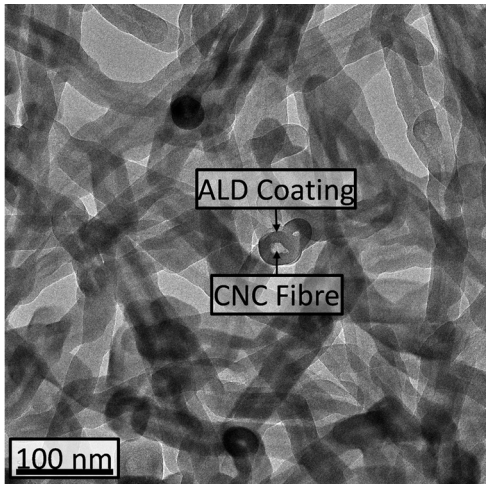


FIG. 2. Cross sectional TEM image of a CNC aerogel coated with 50 cycles of ALD Al_2O_3 using 500 ms pulses and 120 s exposures and purges. This lift-out was taken near the aerogel surface.

aerogel was broken at a depth of approximately 550 μm, and thus, penetration may have exceeded 550 μm in this sample.

In Fig. 3(b) and the higher magnification inset 3(c), each ALD cycle consisted of shorter 20 ms pulses and only 30 s exposures and purges. For these conditions, the Al penetrated just 50 μm into the aerogel. Three regions of Al intensity are again apparent: a 20 μm thick outer region with high Al counts, an inner region at a depth of 20–50 μm with decreasing Al counts, and an uncoated interior region. Comparing the two deposition conditions in Figs. 3(a) and 3(b), it is seen that increasing the pulse time from 20 ms to 180 ms and the purge and exposure times from 30 s to 600 s resulted in approximately a 10× greater penetration of the ALD coating into the aerogel.

The three distinct regions in each of the EPMA images are in agreement with simulation results. Shown in Fig. 3(d) are simulated plots of fiber radius versus penetration depth

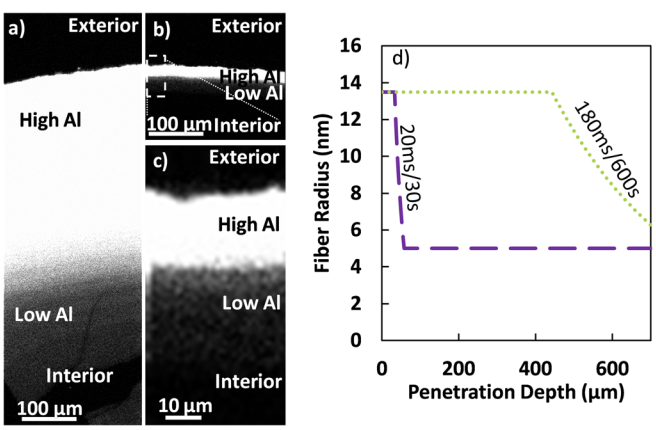


FIG. 3. (Color online) Cross-sectional EPMA images of CNC aerogels coated with 50 cycles of ALD Al_2O_3 at 150 °C using either (a) 180 ms pulses with 600 s exposures and N_2 purges or [(b) and (c)] 20 ms pulses with 30 s exposures and N_2 purges. Image in (c) is a zoomed in view of (b). Shown in (d) is a plot of simulated fiber radius vs depth for both of these conditions. The plateau (cycle limited) regions in (d) correspond to the high Al regions and the decreasing (penetration limited) regions correspond to the low Al regions in the EPMA images.

for aerogels coated with 50 cycles of ALD Al_2O_3 at 150 °C using either 180 ms pulses and 600 s exposures and purges [same as Fig. 3(a)] and 20 ms pulses and 30 s exposures and purges [same as Fig. 3(b)]. The fiber radius is modeled as the initial uncoated fiber radius plus 0.17 nm GPC within the simulated precursor penetration depth. (The aerogel fiber–center to fiber–center spacing used in the precursor penetration model is 100 nm, based on the experimental profiles for 272 cycles with the same conditions shown in Fig. 5.) As the fiber radius increases with each ALD cycle, porosity is reduced and diffusion inhibited, decreasing the simulated precursor penetration depth, L, and leading to three distinct regions in the fiber radius versus penetration depth profile, as described above. The near-surface cycle-limited region, where fiber radius is only a function of the number of ALD cycles, corresponds to the high Al count region in Figs. 3(a)–3(c). The transition or penetration-limited region, in which fiber radius decreases with depth corresponds to the low Al count region in Figs. 3(a)–3(c). Finally, the uncoated region corresponds to the no Al count region deep in the interior. As seen in Fig. 3(d), the depth of both the cycle and penetration limited regions is predicted to increase for the longer pulse and exposure/purge times as there is a larger number of molecules available to coat the surface and more time for the molecules to travel into the aerogel. This is also in agreement with the EPMA data.

Shown in Fig. 4 are cross-sectional SEM images of CNC aerogels coated with 272 cycles of Al_2O_3 using (a) 20 ms pulses and 30 s exposures and purges at 150 °C, (b) 180 ms pulses and 600 s exposures and purges at 150 °C, and (c) 1000 ms pulses and 600 s exposures and purges at 80 °C. 272 cycle coatings are used to produce larger fiber radii for easier SEM imaging. Insets in each low magnification image are higher magnification images taken at various depths from the surface of the aerogel. For Fig. 4(a) the insets are at (i) 10 μm, (ii) 45 μm, and (iii) 70 μm. For Fig. 4(b), the insets are at (i) 50 μm, (ii) 120 μm, and (iii) 300 μm. For Fig. 4(c) the insets are at (i) the surface, (ii) 390 μm, and (iii) 1220 μm. These images show that the coated aerogels have larger diameter fibers and lower porosity near the surface than deeper inside, confirming that the ALD coating is thicker near the surface than deeper inside. The transition to a more open morphology (smaller fiber diameters) occurs deeper into the aerogel with increased pulse times [compare Fig. 4(b) with Fig. 4(a)] and with increased exposure and purge time [compare Fig. 4(c) with Fig. 4(b)].

Shown in Fig. 5 is a plot of SEM measurements (symbols) and simulations (dashed lines) of fiber radius versus depth into the aerogel for the samples from Fig. 4: CNC aerogels coated with 272 cycles of Al_2O_3 using either 20 ms/30 s, 180 ms/600 s, or 1000 ms/600 s pulse/exposure times, respectively. The measured profiles of the 180 ms/600 s and 20 ms/30 s samples appear to be fully penetration limited whereas the 1000 ms/600 s sample appears to be cycle-limited to a depth of 500 μm and penetration-limited beyond that.

To model the 180 ms/600 s and 20 ms/30 s profiles, a fiber spacing of 100 nm, a GPC of 0.17 nm, and an uncoated fiber

Redistribution subject to AVS license or copyright; see http://scitation.aip.org/termsconditions. Download to IP: 128.193.163.187 On: Fri, 08 Aug 2014 20:06:11

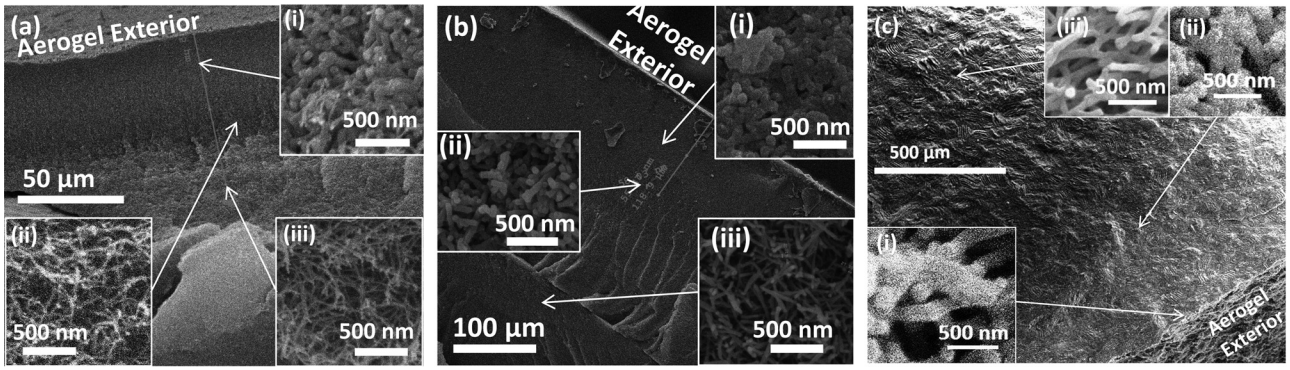


FIG. 4. SEM images of fracture cross sectioned CNC aerogels coated with 272 cycles of Al_2O_3 using either (a) 20 ms pulses and 30 s exposures and purges at 150 °C, (b) 180 ms pulses and 600 exposures and purges at 150 °C, or (c) 1000 ms pulses and 600 s exposures and purges at 80 °C. Insets show morphology for (a) at (i) 10 μm, (ii) 45 μm, and (iii) 70 μm; for (b) at (i) 50 μm, (ii) 120 μm, and (iii) 300 μm; and for (c) at (i) 10 μm, (ii) 390 μm, and (iii) 1220 μm from the surface.

radius of 4 nm (from Fig. 2) are used. These same parameters are used to model the 50 cycle profiles in Fig. 3. The CNC fibers in the 1000 ms/600 s sample are more openly spaced than in the other samples and reached a radius of up to 70 or 80 nm, well above the 40 or 50 nm radius, which appeared to fully close off the porosity in the other samples. To model the 1000 ms/600 s profile, a fiber spacing of 160 nm, a GPC of 0.22 nm, and the same uncoated fiber radius of 4 nm are used. Note that the GPC values for all three conditions, determined from Si witness wafers, are well above the 0.1 nm GPC typically observed for planar ALD Al_2O_3, suggesting that there is some CVD component. One possible explanation is that the purge times used are inadequate and the porous aerogel acted as a virtual leak of reactants into the chamber, leading to CVD and increased GPC. It is observed that a TMA only deposition run with no water intentionally introduced into the chamber resulted in a thin, approximately 6 nm thick coating on the aerogels. Examining Fig. 5, it is apparent that the simulations capture well the trends in the measured thickness profiles. For the 1000 ms/600 s data, the diameter of the aerogel sample is only about 3 mm, and it is

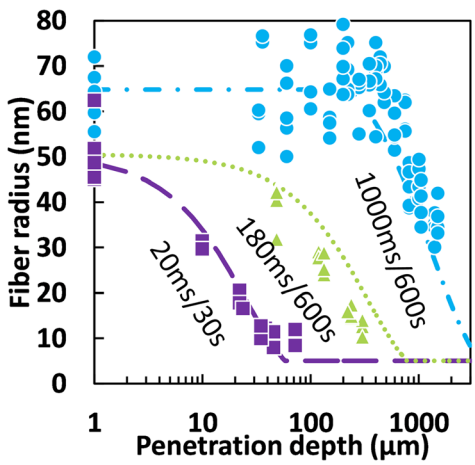


FIG. 5. (Color online) Measured (symbols) and simulated (lines) plots of fiber radius vs depth from the surface for aerogels coated with 272 cycles of Al_2O_3 using 20 ms pulses and 30 s exposures/purges at 150 °C, 180 ms pulses and 600 s exposures/purges at 150 °C, and 1000 ms pulses and 600 s exposures/purges at 80 °C.

coated all the way through the interior so that the fiber radius in the middle is about 40 nm, well above the uncoated fiber radius.

Comparing Figs. 3 and 5, it is seen that using 272 ALD cycles instead of 50 cycles resulted in a greater reduction in L, causing the penetration limited region to dominate the final thickness profile.

B. Decomposition testing

To evaluate the effectiveness of ALD Al_2O_3 coatings in preventing weight loss at elevated temperatures in oxidizing environments, TGA weight loss measurements are performed in air on whole (unbroken after ALD coating) pieces of CNC aerogel. Shown in Fig. 6(a) is a plot of the remaining weight fraction versus temperature for an uncoated CNC aerogel and several CNC aerogels coated with ALD Al_2O_3 under various deposition conditions. In general, it is seen that total weight loss at 450 °C is reduced as the pulse time (dose) and exposure/purge times (diffusion time) are increased. This reduction is largely because as the pulse and exposure/purge times are increased, the CNC aerogels become more fully coated with Al_2O_3, increasing the fraction of the total mass composed of noncombustible Al_2O_3. The "knee" or initial slope change in each curve corresponds to the decomposition onset temperature (T_{onset}) at which significant breakdown of the aerogel begins. The shift of the T_{onset} knee to higher temperatures with longer pulses and purge/exposures indicates that, rather than just adding noncombustible mass, the more complete Al_2O_3 coatings better protect the aerogel from oxidation. To better assess T_{onset}, a plot of the log differential weight % versus temperature for the same data is shown in Fig. 6(b). T_{onset} is taken as the crossing point between the downward sloping baseline and a linear extrapolation of the initial upward slope. As seen in Fig. 6(b), T_{onset} increases with increasing pulse time. This trend may be observed more clearly in Fig. 7.

Shown in Fig. 7 are multiple plots of the average T_{onset} versus (a) pulse time for various exposure and purge times, (b) exposure and purge time for various pulse times, and (c) number of ALD cycles. Figure 7(d) shows T_{onset} versus wt. % Al_2O_3 (the weight gain during ALD divided by

Redistribution subject to AVS license or copyright; see http://scitation.aip.org/termsconditions. Download to IP: 128.193.163.187 On: Fri, 08 Aug 2014 20:06:11

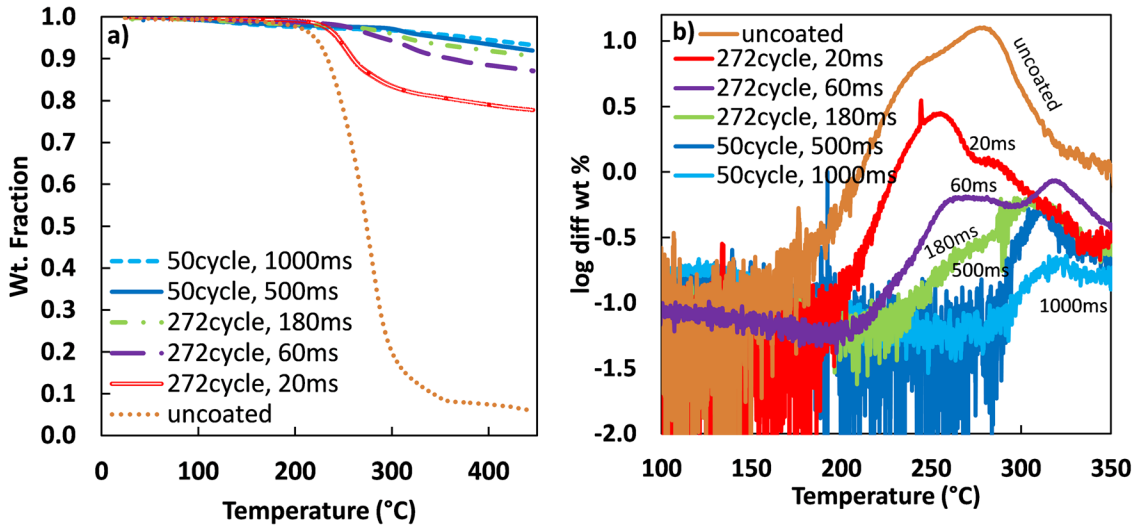


FIG. 6. (Color online) (a) TGA weight fraction vs temperature curves for CNC aerogels coated with ALD Al_2O_3 with various numbers of cycles and pulse times and 120 s exposure and purge times along with an uncoated reference CNC aerogel sample. (b) Log linear plot of differential weight % vs temperature for the same data.

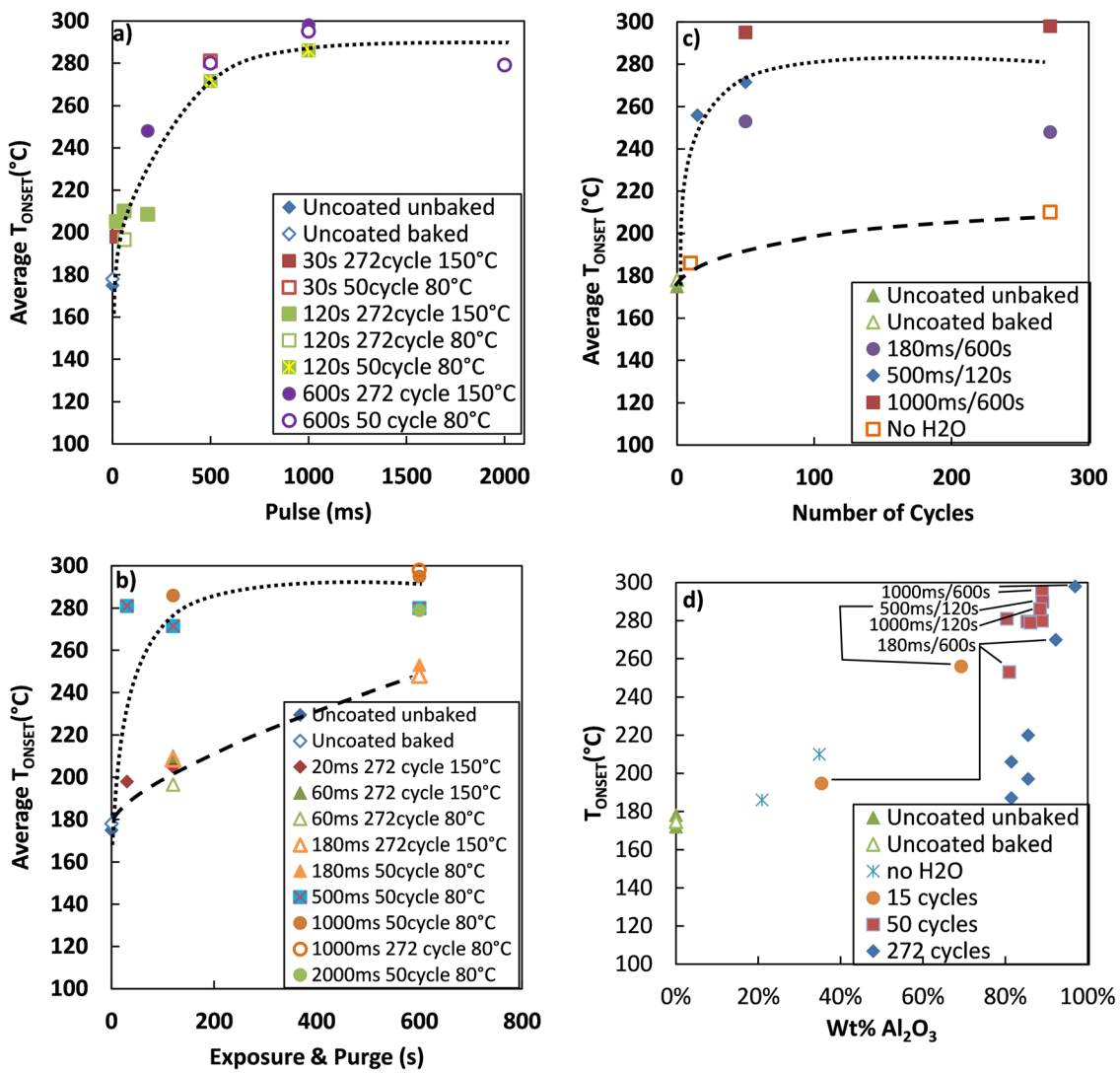


FIG. 7. (Color online) Plot of T_{onset} vs (a) pulse time for various purge and exposure times; (b) exposure and purge time for various pulse times, where the dotted and dashed lines follow the long and short pulse time samples, respectively; (c) number of ALD cycles for various conditions, where the dotted and dashed lines follow the samples deposited with and without H_2O pulses, respectively; and (d) wt. % Al_2O_3. Note that the lines serve only to guide the eye.

Redistribution subject to AVS license or copyright; see http://scitation.aip.org/termsconditions. Download to IP: 128.193.163.187 On: Fri, 08 Aug 2014 20:06:11

post-ALD weight). In general the T_{onset} improves roughly with pulse time, exposure/purge time, ALD cycles, and ash content. Overall, T_{onset} may be increased from ~175 °C for uncoated aerogels up to ~295 °C for aerogels coated with ALD Al_2O_3. Note that the 150 °C vacuum bake out (uncoated, baked) prior to deposition caused no significant change in T_{onset}.

Looking more closely first at Fig. 7(a), it is seen that T_{onset} increases with pulse time (dose) appearing to saturate above 1000 ms. In Fig. 7(b), it is seen that for large doses (pulse times above 500 ms, as roughly indicated by the dotted line), even exposure/purges as short as 30 s may lead to a large increase in T_{onset}. For smaller doses (roughly indicated by the dashed line), the improvement in T_{onset} is not as great, and T_{onset} exhibits a greater dependence on exposure/purge time. Overall, depositions with large doses (pulse times), even with modest purge and exposure times, offer the best improvement in T_{onset}, likely because they effectively coat the largest portion of the aerogel.

The data in Fig. 7(c) suggest that the thicker 272 cycle coatings do not result in substantial improvement in T_{onset} over the thinner 50 cycle coatings. It also can be seen that TMA only depositions (without intentionally introduced water vapor) also provide a slight increase in T_{onset} as might be expected from a thin layer of Al_2O_3. As discussed above, the deposition of ~6 nm Al_2O_3 during the nominally TMA-only deposition may be due to residual water vapor trapped in the aerogel.

Figure 7(d) shows that T_{onset} increases roughly with the weight percent Al_2O_3 (wt. %, ALD mass/total mass). However, it is seen that the depositions that add the most Al_2O_3 do not necessarily provide the greatest improvement in T_{onset}. For example, many of the 272 cycle coatings (blue diamonds) show reduced improvement in T_{onset} as compared to the 50 cycle depositions (red squares) with comparable wt. % Al_2O_3. This is likely because the thickness deposited by the 50 cycle coatings is already sufficient to protect the aerogel, whereas the additional cycles in the 272 cycle coatings preferentially add more mass near the surface as the porosity of the aerogel is closed off for the thicker coatings. This extra mass increases wt. % Al_2O_3 without improving T_{onset}. The best improvements in T_{onset} are provided by the 50 cycle films with optimum dose and purge/exposure conditions so as to minimize excess Al_2O_3 deposition.

IV. CONCLUSIONS

CNCs are renewable fibers with promising mechanical properties, but the low temperature at which degradation occurs due to oxidation limits their use as reinforcing fillers in polymers with melt temperatures above roughly 175 °C. In this work, we formed an organic/inorganic nanocomposite by conformally coating CNC aerogel scaffolds with thin layers of Al_2O_3 via ALD. SEM results showed Al_2O_3 penetration of greater than 1500 μm for appropriate ALD dose, exposure, and purge conditions. SEM images showed that Al_2O_3 coatings are conformal throughout the aerogel but decrease in thickness as a function of depth from the aerogel surface, suggesting that the penetration depth of successive ALD cycles decreases as the film is grown. A reduction in penetration depth with successive cycles is in agreement with trends predicted by simulation models, indicating that the decrease in penetration depth is due to the reduction of CNC aerogel porosity caused by the ALD coating increasing the radius of the CNC fibers. TGA showed that the Al_2O_3 coatings are effective in increasing the decomposition onset temperature, T_{onset}, of CNC aerogels, and that more completely coated aerogels are better protected against oxidation. For the best coatings, we found that T_{onset} is increased by 120 °C, from 175 °C to 295 °C. Based on our results, it is anticipated that the hard, wear-resistant Al_2O_3 coating and increased allowable processing temperature should allow coated aerogels to be incorporated into a wide variety of polymers, resulting in polymer/Al_2O_3 coated CNC aerogel composites with improved mechanical properties. Combined with the renewable nature of CNCs, these improved properties may make ALD coated CNC aerogel composites an attractive alternative as a reinforcing filler in polymers. Future work will focus on the addition of coated CNC aerogels into polymers to form composites. Finally, CNC aerogels are electron beam sensitive and thus difficult to image. We have found that even a thin ALD Al_2O_3 coating greatly improves the stability of the aerogel structure when exposed to an electron beam and we anticipate that thin ALD Al_2O_3 coatings will enable improved fundamental studies of the process-microstructure relationships in these aerogels.

ACKNOWLEDGMENTS

EPMA was carried out at the Electron Microprobe Laboratory in the College of Oceanic and Atmospheric Sciences at OSU. The authors acknowledge Yi Liu, Peter Eschbach, and Teresa Sawyer of the OSU Electron Microscopy Facility supported by the NSF MRI grant # 1040588, the Murdock Charitable Trust and the Oregon Nanoscience and Microtechnologies Institute, as well as Skip Rochefort for use of TGA and C. Tasker of the OSU Materials Synthesis and Characterization (MaSC) Facility for equipment support. J. F. Conley, Jr., was supported by NSF DMR 0805372, S. W. Smith was supported by NSF CHE 1102637, J. Simonsen and C. Buesch were supported by a joint venture agreement with the USDA Forest Products Lab.

[1]R. J. Moon, A. Martini, J. Nairn, J. Simonsen, and J. Youngblood, Chem. Soc. Rev. **40**, 3941 (2011).
[2]C. Rong-shi, W. Neng, D. En-young, and X. Feng, J. South China Univ. Technol. **35**, 91 (2007), available at http://202.38.194.234/zrb/EN/abstract/abstract10419.shtml.
[3]L. Heath and W. Thielmans, Green Chem. **12**, 1448 (2010).
[4]J. Biener, T. F. Baumann, Y. Wang, E. J. Nelson, S. O. Kucheyev, W. V. Hamza, M. Kemell, M. Ritala, and M. Leskelä, Nanotechnology **18**, 055303 (2007).
[5]S. Ghosal, T. F. Baumann, J. S. King, S. O. Kucheyev, Y. Wang, M. A. Worsley, J. Biener, S. F. Bent, and A. V. Hamza, Chem. Mater. **21**, 1989 (2009).
[6]J. W. Elam, J. A. Libera, M. J. Pellin, A. V. Zinovev, J. P. Greene, and J. A. Nolen, Appl. Phys. Lett. **89**, 053124 (2006).
[7]S. O. Kucheyev *et al.*, Appl. Phys. Lett. **86**, 083108 (2005).

Redistribution subject to AVS license or copyright; see http://scitation.aip.org/termsconditions. Download to IP: 128.193.163.187 On: Fri, 08 Aug 2014 20:06:11

[8]T. C. Li, F. Fabregat-Santiago, O. K. Farha, A. M. Spokoyny, S. R. Raga, J. Bisquert, C. A. Mirkin, T. J. Marks, and J. T. Hupp, J. Phys. Chem. C **115**, 11257 (2011).
[9]R. L. Puurunen, J. Appl. Phys. **97**, 121301 (2005).
[10]G. K. Hyde *et al*., Langmuir **26**, 2550 (2010).
[11]J. S. Jur, W. J. Sweet III, C. J. Oldham, and G. N. Parsons, Adv. Funct. Mater. **21**, 1993 (2011).
[12]G. K. Hyde, S. D. McCullen, S. Jeon, S. M. Stewart, H. Jeon, E. G. Loboa, and G. N. Parsons, Biomed. Mater. **4**, 025001 (2009).
[13]E. Ghadiri, N. Taghavinia, S. M. Zakeeruddin, M. Grätzel, and J. E. Moser, Nano Lett. **10**, 1632 (2010).
[14]J. T. Korhonen, P. Hiekkataipale, J. Malm, M. Karppinen, O. Ikkala, and R. H. A. Ras, ACS Nano **5**, 1967 (2011).
[15]J. T. Korhonen, M. Kettunen, R. H. A. Ras, and O. Ikkala, ACS Appl. Mater. Interfaces **3**, 1813 (2011).
[16]N. T. Cervin, C. Aulin, P. T. Larsson, and L. Wågberg, Cellulose **19**, 401 (2012).
[17]M. Kettunen *et al*., Adv. Funct. Mater. **21**, 510 (2011).
[18]P. F. Carcia, R. S. Mclean, B. B. Sauer, and M. H. Reilly, J. Nanosci. Nanotechnol. **11**, 7994 (2011).
[19]A. K. Roy, W. Baumann, S. Schulze, M. Hietschold, T. Mäder, D. J. Nestler, B. Wielage, and W. A. Goedel, J. Am. Ceram. Soc. **94**, 3604 (2011).
[20]A. Yanguas-Gil and J. W. Elam, ECS Trans. **41**, 169 (2011).
[21]S. Montanari, M. Roumani, L. Heux, and M. R. Vignon, Macromolecules **38**, 1665 (2005).
[22]S. Noorani, J. Simonsen, and S. Atre, *ACS Symposium Series*, edited by K. Oksman and M. Sain (American Chemical Society, Washington, D.C., 2006), Vol. 938, p. 209.
[23]A. C. Besemer, A. E. J. de Nooy, and H. van Bekkum, *Cellulose Derivatives ACS Symposium Series*, edited by T. J. Heinze and W. G. Glasser (Washington, D.C., 1998), Vol. 668, p. 73.
[24]P. L. Bragd, A. C. Besemer, and H. van Bekkum, J. Mol. Catal. A: Chem. **170**, 35 (2001).
[25]A. E. J. de Nooy, A. C. Besemer, and H. van Bekkum, Carbohydr. Res. **269**, 89 (1995).
[26]A. E. J. de Nooy, A. C. Besemer, H. van Bekkum, J. A. P. P. van Dijk, and J. A. M. Smit Macromolecules **29**, 6541 (1996).
[27]R. G. Gordon, D. Hausmann, E. Kim, and J. Shepard, Chem. Vap. Deposition **9**, 73 (2003).
[28]G. W. Scherer, J. Non-Cryst. Solids **225**, 192 (1998).

Redistribution subject to AVS license or copyright; see http://scitation.aip.org/termsconditions. Download to IP: 128.193.163.187 On: Fri, 08 Aug 2014 20:06:11